Chemical Science

ROYAL SOCIETY OF CHEMISTRY

EDGE ARTICLE

View Article Online
View Journal | View Issue

Cite this: *Chem. Sci.*, 2022, **13**, 9202

All publication charges for this article have been paid for by the Royal Society of Chemistry

Received 31st May 2022
Accepted 7th July 2022

DOI: 10.1039/d2sc03028d

rsc.li/chemical-science

Direct observation of reversible bond homolysis by 2D EXSY NMR†

Satoshi Takebayashi, *[a] Robert R. Fayzullin [b] and Richa Bansal [a]

Bond homolysis is one of the most fundamental bond cleavage mechanisms. Thus, understanding of bond homolysis influences the development of a wide range of chemistry. Photolytic bond homolysis and its reverse process have been observed directly using time-resolved spectroscopy. However, direct observation of reversible bond homolysis remains elusive. Here, we report the direct observation of reversible Co–Co bond homolysis using two-dimensional nuclear magnetic resonance exchange spectroscopy (2D EXSY NMR). The characterization of species involved in this homolysis is firmly supported by diffusion ordered NMR spectroscopy (DOSY NMR). The unambiguous characterization of the Co–Co bond homolysis process enabled us to study ligand steric and electronic factors that influence the strength of the Co–Co bond. Understanding of these factors will contribute to rational design of multimetallic complexes with desired physical properties or catalytic activity.

Introduction

Bond homolysis and heterolysis are the most common mechanisms for the cleavage of covalent bonds. Therefore, a fundamental understanding of these mechanisms is important for the development of a wide range of chemistry. Many studies have been reported to understand the fundamental aspects of bond homolysis, and studies are ongoing to utilize this process in a variety of chemistry, biology, and interplay of them,[1] including catalysis,[2,3] natural product synthesis,[4] polymer[5] and material chemistry.[6,7] The majority of bond homolysis reactions are irreversible reactions that favour the formation of covalent bonds. However, it is known that steric crowding around the radical center and delocalization of spin density shift this equilibrium towards the generation of persistent radical species,[8] and by virtue of this stabilization, many radical species have been isolated.[7,9,10] Conventionally (Fig. 1a), reversible bond homolysis has been studied most frequently using a temperature-dependent reversible change of UV-Vis,[11–22] IR,[15,23,24] EPR,[17,18,20–22,25–29] or NMR[16–18,21–24,30–37] spectra. In a few cases, reversible bond homolysis has been observed in the solid state by powder X-ray diffractometry.[38–40] Direct observation of photolytic bond homolysis and irreversible recombination and/or decomposition of transient radical species has been reported in detail.[41–45] However, direct spectroscopic detection of reversible bond homolysis remains elusive.

Two-dimensional NMR exchange spectroscopy[46–48] (2D EXSY NMR) and 2D IR[49–52] spectroscopy are unique methods to detect real-time chemical exchange as exchange signals. A large variety of chemical exchanges with a wide range of exchange time scales have been studied using these methods;[48,51] however, their application in direct observation of reversible bond homolysis is unknown (Fig. 1b). A possible reason for this lack of observation is the incompatibility of the exchange rates of reversible bond homolysis. Thus, reversible bond homolysis is too slow to be observed using a 2D IR method.[53,54] In contrast, it is usually too fast to obtain resolved NMR signals from both the radical species and dimer of the radical species at NMR compatible temperatures (−150 to 150 °C).[18,32,33]

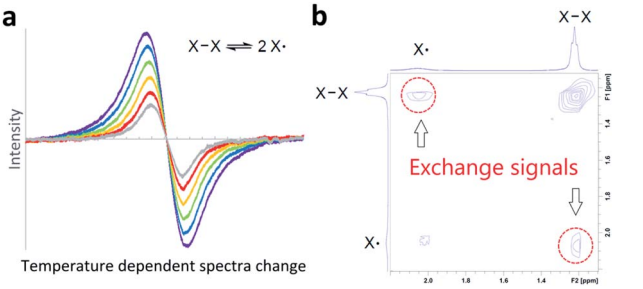

Fig. 1 Methods to observe and prove reversible bond homolysis. (a) A conventional method: temperature-dependent reversible change of spectra. (b) This work: direct observation of exchange signals by 2D EXSY NMR.

[a]*Science and Technology Group Okinawa Institute of Science and Technology Graduate University 1919-1 Tancha, Onna-son, Okinawa 904-0495, Japan. E-mail: satoshi.takebayashi@oist.jp*

[b]*Arbuzov Institute of Organic and Physical Chemistry, FRC Kazan Scientific Center, Russian Academy of Sciences, 8 Arbuzov Street, Kazan 420088, Russian Federation*

† Electronic supplementary information (ESI) available: Synthetic details, spectroscopic and X-ray diffraction data (pdf). Raw data used for the van't Hoff plot (excel). Raw data used for the Eyring plot (excel). CCDC 2165654–2165661. For ESI and crystallographic data in CIF or other electronic format see https://doi.org/10.1039/d2sc03028d

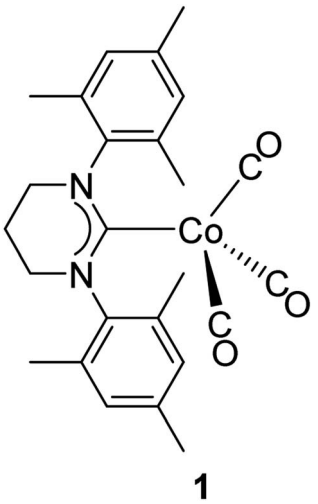

1

Fig. 2 Isolable Co-metalloradical **1**.

Few reports[24,37,55] are known where the exchange rates are slow enough to resolve monomeric and dimeric species in an NMR spectrum. However, real-time 2D EXSY NMR observation of exchange between these monomers and dimers has not been reported, possibly due to the broadening of NMR signals caused by paramagnetic radical species. Therefore, in theory, if the rate of reversible bond homolysis is slow and sufficiently sharp NMR signals from both paramagnetic radical species and diamagnetic radical dimers are detectable, direct observation of reversible bond homolysis is possible using 2D EXSY NMR.

Recently, we have isolated formal 17-electron Co(0) metalloradical complex **1** utilizing a bulky ring-expanded *N*-heterocyclic carbene (reNHC) ligand (Fig. 2).[56] This class of Co(0) carbonyl complexes usually exists as dimers to fulfill the formal 18-electron configuration; however, **1** was isolated as a monomer as the bulky reNHC ligand prevents dimerization. Furthermore, some of the ^{1}H NMR signals from **1** were relatively sharp (linewidth at half maximum < 100 Hz). From this finding, we envisioned that direct 2D EXSY NMR observation of reversible bond homolysis is possible if less bulky NHC ligands, which promote reversible homolysis of Co–Co bonds, were employed. Here, we report the direct observation of reversible Co–Co bond homolysis using 2D EXSY NMR.

Results and discussion

Preparation and characterization of a cobalt dimer

At the onset of this study, 1,3-bis(2,4,6-trimethylphenyl)-4,5-dihydroimidazol-2-ylidene (SIMes) was chosen as a less bulky NHC ligand with respect to the ring-expanded analog in **1** since the steric bulk of NHC ligands is known to increase by increasing the ring size of the NHC ligands.[57–61] The reaction between SIMes and $Co_2(CO)_8$ formed dimeric cobalt complex **2-Mes** in a 95% yield (Fig. 3a). The diamagnetic complex **2-Mes** was characterized using single-crystal X-ray diffractometry (SC-XRD), ^{1}H, ^{13}C{^{1}H}, and 2D NMR, FTIR, and UV-Vis spectroscopy, and elemental analysis. The SC-XRD structures of **2-Mes**

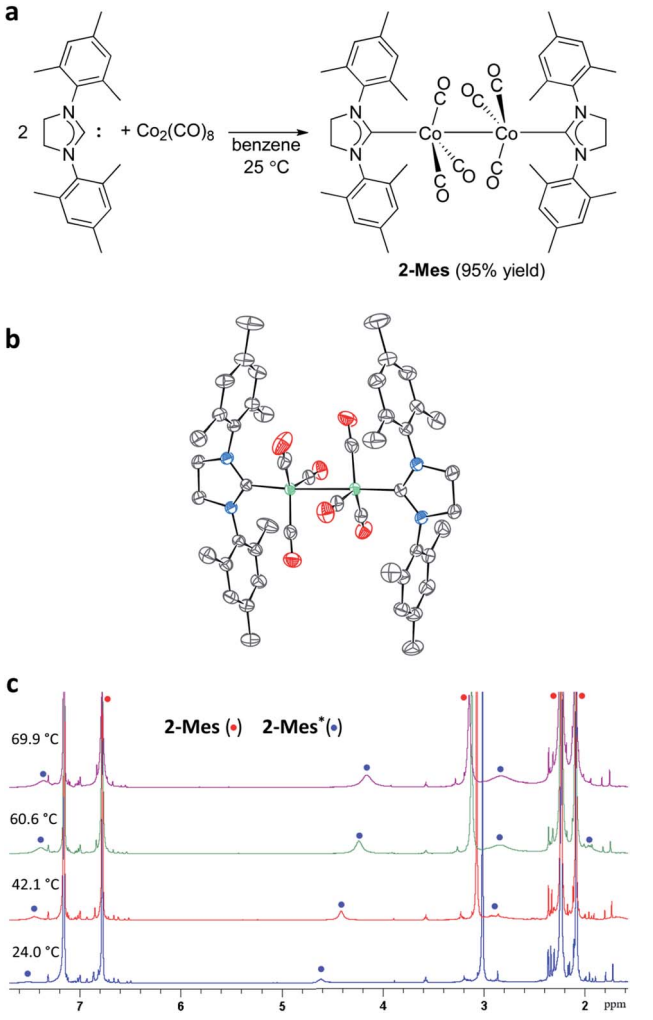

Fig. 3 Preparation and characterization of **2-Mes**. (a) Preparation of **2-Mes**. (b) SC-XRD structure of **2-Mes** with 80% thermal ellipsoids. Hydrogen atoms, solvent molecules, and the second crystallographically independent **2-Mes** molecule are omitted for clarity. (c) Variable temperature ^{1}H NMR spectra (500 MHz, C_6D_6) of **2-Mes** showing the increasing concentration of radical species **2-Mes*** on increasing the temperature.

revealed a dimeric structure with a long Co–Co bond of 2.71989(18) Å, which is one of the longest Co(0)–Co(0) bonds known[62,63] due to the steric effect of the SIMes ligand (Fig. 3b). There is another crystallographically independent, centrosymmetric molecule of **2-Mes** in the same unit cell; however, the Co–Co bond length of this molecule is even longer (2.7520(2) Å). The presence of a Co–Co bond is also supported by UV-Vis absorption at 369 nm. This absorption was assigned as a σ–σ^* transition of the Co–Co bonds based on a previous report.[64] At first glance, sharp, intense ^{1}H and ^{13}C{^{1}H} NMR signals from **2-Mes** at 24.0 °C support a diamagnetic, dimeric structure in a solution as observed in the solid state (Fig. 3c). However, a close inspection of the ^{1}H NMR spectra revealed the presence of a small broad signal at 4.62 ppm in all batches of **2-Mes** (Fig. 3c). Initially, we assumed this species (**2-Mes***) to be a trace impurity in **2-Mes** since the relative integration of this species

was roughly 30 times smaller than that of **2-Mes**. However, we found that the intensity of this signal increased reversibly with increasing temperature. Thus, in C_6D_6, the initial 1 : 30 ratio at 24.0 °C changed to a 1 : 3 ratio at 69.9 °C, along with a significant broadening of signals from **2-Mes** (Fig. 3c). In comparison, no broadening of the residual C_6D_6 signal was observed. Four very broad ^{1}H NMR signals were detectable at 60.6 °C; however, an accurate integration ratio could not be obtained due to signal overlapping and broadening. Monitoring of magnetic susceptibility of C_6D_6 solution of **2-Mes** using Evans' method also revealed a reversible increase of magnetic susceptibility with increasing temperature (Table S1†). Thus, paramagnetic species is formed on heating.

Characterization of the paramagnetic species 2-Mes*

The identity of the paramagnetic species **2-Mes** was confirmed by several control experiments and spectroscopic observations. First, trapping of the paramagnetic species by 2,2,6,6-tetramethylpiperidine-1-oxyl (TEMPO) resulted in the formation of TEMPO adducts **3** (Fig. 4a). This result suggests homolysis of the Co–Co bond in **2-Mes** based on analogous reactivity between the isolated cobalt radical **1** and TEMPO.[56] Second, the ^{1}H NMR spectra showed that the formation of **2-Mes*** is not accompanied by the formation of a free SIMes ligand, and hence, dissociation of the SIMes ligand is not involved in this process. Third, the formation of **2-Mes*** is not affected by the presence of CO pressure (3 bar) (Fig. S44†). Thus, dissociation of the CO ligand is also not involved in the formation of **2-Mes***. Fourth, the **2-Mes***/**2-Mes** ratio increases with increasing dilution of the solution (Table S2†). This observation is consistent with the favored formation of monomeric species in a dilute solution. Fifth, the EPR measurement of the C_6D_6 solution of **2-Mes** at 20 to 62 °C showed the presence of a cobalt-centered radical species with an isotropic g-value of 2.08. The observed isotropic g-value is the same as the one observed for isolated Co radical **1**.[56] As in the case of the NMR observations, EPR signal intensity increased reversibly with increasing temperature (Fig. 4b and S46†). Variable temperature UV-Vis spectroscopy revealed a reversible decrease or increase of the Co–Co σ–σ* transition absorption band at 369 nm on increasing or decreasing the solution temperature, respectively[12] (Fig. 4c and S47†). Thus, the Co–Co bond cleaves reversibly according to temperature change. Collectively, these observations support the temperature-dependent formation of a cobalt-centered radical *via* the cleavage of the Co–Co bond in **2-Mes**. Finally, the characterization of **2-Mes*** was strongly supported by 2D diffusion ordered NMR spectroscopy[65] (2D DOSY NMR) measurement of a mixture of **2-Mes** and **2-Mes*** in the presence of [Ni(SIMes)(CO)$_3$](**4**)[66] as an internal standard (Fig. 4d). The molecular weight (449.17 g mol^{-1}), tetrahedral geometry, and

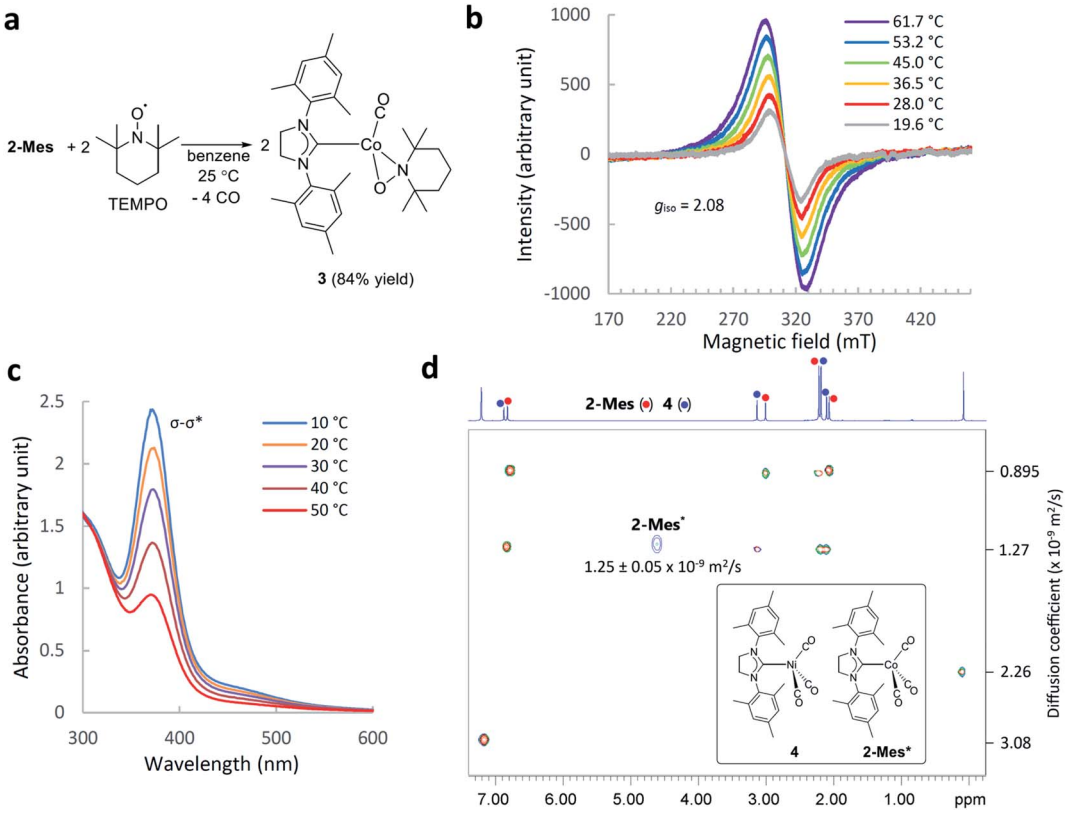

Fig. 4 Characterization of **2-Mes***. (a) Trapping of **2-Mes*** by TEMPO. (b) Variable temperature EPR spectra (X-band, in C_6D_6) of **2-Mes***. (c) Change of UV-Vis spectra (in C_6H_6) of a mixture of **2-Mes** and **2-Mes*** on increasing the temperature from 10 to 50 °C. (d) 2D DOSY NMR spectrum (500 MHz, C_6D_6, 24.0 °C) of an equilibrium mixture of **2-Mes** and **2-Mes*** in the presence of **4** and hexamethyldisiloxane (a signal at around 0 ppm) as internal standards.

charge neutrality of **4** make this molecule the closest structural analog to the tetrahedral[56] and neutral [Co(SIMes)(CO)$_3$] radical (449.41 g mol^{-1}) with practically identical molecular weights. 2D DOSY NMR spectra recorded at 24 °C showed complete sets of signals from **2-Mes** and **4** (Fig. 4d), and one signal from **2-Mes*** at 4.62 ppm due to a lower concentration of **2-Mes*** and broadening of signals from paramagnetic **2-Mes***.[65] A 2D DOSY NMR study revealed that **2-Mes*** (1.25(5) × 10^{-9} m^2 s^{-1}) and **4** (1.27 × 10^{-9} m^2 s^{-1}) have nearly identical diffusion coefficients. Consistent with this observation, the diffusion coefficient of the dimeric complex **2-Mes** (0.895 × 10^{-9} m^2 s^{-1}) was significantly smaller than that of **4** and **2-Mes***. To the best of our knowledge, DOSY NMR characterization of monomeric and dimeric species involved in reversible bond homolysis is unprecedented. Together, these observations strongly support that the paramagnetic species **2-Mes*** is a monomeric [Co(SIMes)(CO)$_3$] radical that is in equilibrium with dimeric **2-Mes**.

Observation of reversible Co–Co bond homolysis by 2D EXSY NMR

With the reliable characterization of both **2-Mes** and **2-Mes*** in hand, 2D EXSY NMR observation of reversible Co–Co bond homolysis was examined. To our delight, the 2D EXSY NMR spectra (46.7 °C, in C_6D_6) of the mixture of **2-Mes** and **2-Mes*** unequivocally showed exchange signals for the homolysis of the Co–Co bond in **2-Mes** (Fig. 5). More specifically, 2D EXSY NMR showed four exchange signals between four ^{1}H signals from **2-Mes** and four ^{1}H signals from **2-Mes***. The phase difference between these exchange signals (black) and the nuclear Overhauser effect (NOE) signals (red) clearly showed that these signals are due to an exchange between **2-Mes** and **2-Mes***. Consistent with the 2D EXSY NMR observation, the ^{1}H NMR signals from **2-Mes** and **2-Mes*** broadened upon increasing the temperature and merged into four broad signals at 137 °C (recorded in toluene-d_8 under 5 bar N_2) (Fig. S48†).

2D EXSY NMR enabled us to assign all ^{1}H NMR signals from paramagnetic **2-Mes***, and hence concentration ratios between **2-Mes** and **2-Mes*** were determined at variable temperatures using the integration ratio of ^{1}H NMR signals. The van't Hoff plot (Fig. 6) based on the obtained ratio of **2-Mes** and **2-Mes*** revealed an experimental Co–Co bond dissociation enthalpy (BDE) of 20.4(2) kcal mol^{-1}, entropy (ΔS°) of 50.1(7) cal mol^{-1} K^{-1} (averages of three independent measurements and standard deviations in brackets), and bond dissociation free energy (BDEF) of 5.5 ± 0.02 kcal mol^{-1}. The observed BDE is within the range of the reported Co–Co BDE of $Co_2(CO)_8$ (19(2) or 20(7) kcal mol^{-1}).[32,67] The observed large positive ΔS° is in line with other bond homolysis processes.[12,18,21,23,25,29,32–34,37,55] It is proposed that ΔS° increases with increasing steric factors due to more restricted metal–metal bond rotation.[23,25]

BDE and ΔS° for the homolysis of the Co–Co bond in **2-Mes** were also determined by double integration of variable temperature EPR spectra using a solution of **1** as an external standard (see the ESI for more details). The van't Hoff plot based on the EPR measurement in C_6D_6 gave a BDE of 20.3(5) kcal mol^{-1} and ΔS° of 48.2(17) cal mol^{-1} K^{-1} (averages and standard deviations of two independent measurements). These values are consistent with BDE and ΔS° determined by the NMR method. A Co–Co BDFE of 5.5 ± 0.02 kcal mol^{-1} is significantly lower than that of $Co_2(CO)_8$ (10(3) kcal mol^{-1}) despite the relatively large experimental uncertainty of the latter

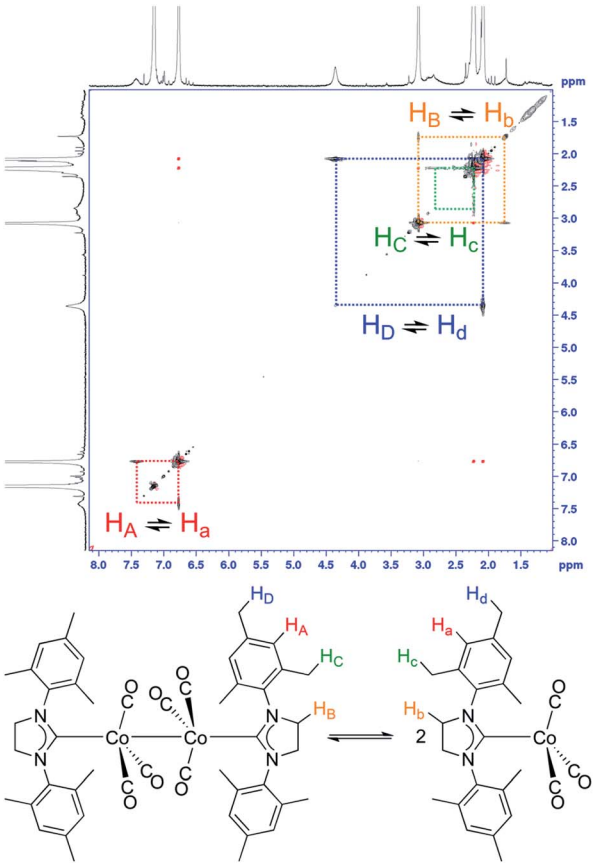

Fig. 5 Direct 2D EXSY NMR observation of Co–Co bond homolysis. 2D EXSY NMR spectra (500 MHz, C_6D_6, 46.7 °C) of an equilibrium mixture of **2-Mes** and **2-Mes***, and assignment of exchanging signals. Red off-diagonal signals are due to NOE.

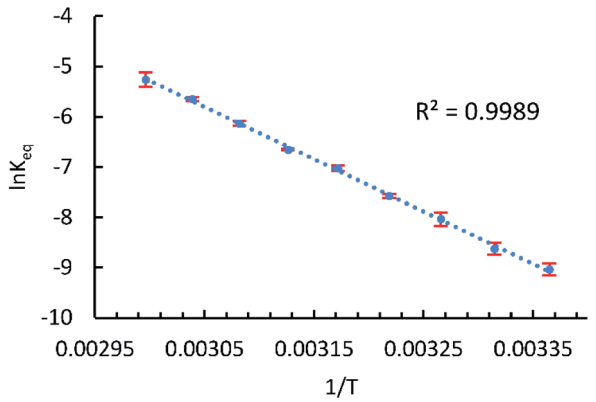

Fig. 6 van't Hoff plot for the Co–Co bond homolysis of **2-Mes** plotted using NMR data. T: temperature (K), K_{eq}: [**2-Mes***]^2/[**2-Mes**] (mol L^{-1}), and error bar: standard deviation of three independent measurements.

value. This large decrease of Co–Co BDFE can be explained by a combination of the bulky NHC ligand and electron donation from the NHC ligand to a Co–Co antibonding orbital.[68]

Elucidation of ligand steric and electronic effects on Co–Co bond strength

The study of metal–metal bonds and their application are currently among the most active areas of study in catalysis,[69,70] and inorganic and organometallic chemistry.[71] The ligand steric effect is a reliable way to control metal–metal bond strength.[13,56,72–74] In contrast, the ligand electronic effect on metal–metal bond strength is not fully understood[23,68,75] partly due to the lack of an appropriate system to study ligand steric and electronic effects separately.[23] Thus, we addressed this question by investigating BDE, ΔS°, and BDFE of Co–Co bond homolysis in several $[Co(NHC)(CO)_3]_2$ complexes (Fig. 7) using our NMR method and systematic change of steric and electronic properties of the NHC ligands.

As in the case of **2-Mes**, in all ^{1}H NMR spectra of $[Co(NHC)(CO)_3]_2$ complexes, one set of sharp diamagnetic signals from $[Co(NHC)(CO)_3]_2$ and another set of broader paramagnetic signals from monomeric $[Co(NHC)(CO)_3]$ species were observed (Fig. S54–59†). The 2D EXSY NMR spectra confirmed exchange between $[Co(NHC)(CO)_3]_2$ and $[Co(NHC)(CO)_3]$. Experimental Co–Co BDE, ΔS°, and BDEF were determined using the van't Hoff plot based on the NMR integration ratio of dimeric and monomeric species. Comparison of thermodynamic parameters between **2-Me**, **2-Et**, and **2-^{i}Pr** revealed a small decrease of BDFE (<1.0 kcal mol^{-1}) upon increasing the steric bulk due to a combination of a slight (<0.8 kcal mol^{-1}) decrease of BDE and a slight increase of ΔS° (<1.1 cal mol^{-1} K^{-1}) (Table 1). This observation is consistent with the study by Watkins *et al.*,[23] where they found that bulkier $[CrCp^*(CO)_3]_2$ (Cp*: pentamethylcyclopentadienyl) has a smaller BDE and larger positive ΔS° than $[CrCp(CO)_3]_2$ (Cp: cyclopentadienyl) for the cleavage of Cr–Cr bonds, even though their study could not separate the contribution from steric and electronic effects.

When the electronic effect of the NHC ligands was examined using **2-Me**, **2-Mes**, **2-Br**, **2-OEt**, and **2-NEt$_2$** (Table 1), a larger decrease of BDFE (<2.6 kcal mol^{-1}) was observed upon increasing electron-donating ability of NHC ligands. In this case, a combination of a larger decrease of BDE (<5.2 kcal mol^{-1}) and a large decrease of ΔS° (<8.6 cal mol^{-1} K^{-1}) resulted in the overall larger decrease of BDFE. From this experiment, we conclude that Co–Co bonds in $[Co(ligand)(CO)_3]_2$ complexes are weakened not only by steric bulk but also by electron donation from the ligand. This conclusion is consistent with the previous argument made by comparing Co–Co bond lengths.[76] It is worth pointing out that Co(III)–alkyl bonds in cobaloxime complexes are strengthened by electron donation from the *trans*-axial ligands.[77] This observation was explained by the fact that homolysis of the Co(III)–alkyl bond involves the reduction of the Co(III) complex to a Co(II) complex that is destabilized in the presence of an electron-donating ligand.[77] Such an oxidation state change is not involved in Co–Co bond homolysis. However, the observed weakening of the Co–Co bond by an electron-donating ligand can be explained by an analogous argument. Thus, stabilization of the electron-deficient, formal 17-electron species by an electron-donating ligand will result in the preferred formation of 17-electron species and consequently weaker Co–Co bonds. Considering that all homolysis of bonds between transition metals forms species with a less formal electron count, we expect that the observed electronic effect is common in bonds between transition metals and can be applicable to rational design of transition metal complexes with various metal–metal bond strengths. Interestingly, in line with our observation, C–C bonds in substituted dicyanomethyl radical dimers are weaker in the presence of electron-donating substituents.[29] We propose that the reported[23,33] weakening of the Cr–Cr bond in $[CrCp^*(CO)_3]_2$ is due to the combination of steric and electronic effects. For comparison, we also examined the ^{1}H NMR spectra of $[Co(PBu_3)(CO)_3]_2$, $[Co(PCy_3)(CO)_3]_2$, and $[Co(P(OAr)_3)(CO)_3]_2$ (Bu: *n*-butyl, Cy: cyclohexyl, Ar: 2,4-di-*tert*-butylphenyl). However, these phosphine analogs did not show signals from monomeric species even at 75 °C. This result is consistent with the crucial role of both steric hindrance[60,78] and electron-donating properties[79,80] of NHC ligands in weakening Co–Co bonds. Indeed, the BDE of a Co–Co bond in $[Co(PBu_3)(CO)_3]_2$ is estimated to be > 23 kcal mol^{-1}.[81]

Examination of the correlation between solid-state Co–Co bond length and BDE revealed a general trend of increasing Co–Co bond length with decreasing BDE. However, an anomalously shorter Co–Co bond was observed in **2-NEt$_2$**, probably due to crystal packing effects. Crystallographically determined metal–metal bond length does not always reflect metal–metal bond strength.[70] We also estimated Gibbs free energy of activation ($\Delta G^\ddagger_{298}$) for the formation of a Co–Co bond (reverse homolysis) using a method based on NMR line broadening.[33,82] In this case, however, all $[Co(NHC)(CO)_3]_2$ complexes studied showed a $\Delta G^\ddagger_{298}$ between 18.1 and 19.2 kcal mol^{-1} with a larger experimental error and no significant steric nor electronic effect on $\Delta G^\ddagger_{298}$ was observed. This observation is consistent with a relatively narrow range of UV-Vis absorption maxima (369–381 nm) that corresponds to the σ–σ^* transition of Co–Co bonds in $[Co(NHC)(CO)_3]_2$ complexes. Thus, rate of Co–Co bond homolysis can be controlled by the relative thermodynamic stability of radical species.

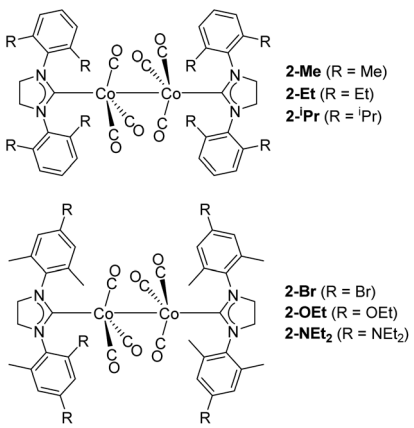

Fig. 7 Structures of $[Co(NHC)(CO)_3]_2$ complexes.

Table 1 Ligand steric and electronic effects on Co–Co homolysis

Complex	Co–Co (Å)[a]	BDE (kcal mol^{-1})[b]	ΔS° (cal mol^{-1} K^{-1})[b]	BDFE (kcal mol^{-1})[b,c]	σ–σ* (nm)[d]	$\Delta G^\ddagger_{298}$ (kcal mol^{-1})[b,e]
2-Me	2.7183(6)	21.1(2)	51.3(7)	5.8 ± 0.01	372	18.1(7)
2-Et	2.7461(4), 2.7492(4)[f]	20.5(2)	50.9(6)	5.3 ± 0.04	372	18.5(1)
2-^{i}Pr	2.7512(3)	20.3(3)	52.0(10)	4.8 ± 0.03	381	18.4(6)
2-Br	2.7153(3)	23.1(4)	53.9(11)	7.0 ± 0.1	371	19.2(3)
2-Mes	2.71989(18), 2.7520(2)[f]	20.4(2)	50.1(7)	5.5 ± 0.02	369	18.5(7)
2-OEt	2.7431(3)	19.3(1)	47.0(3)	5.3 ± 0.06	370	18.9(3)
2-NEt$_2$	2.72357(18)	17.9(5)	45.3(13)	4.4 ± 0.06	364	18.9(1)

[a] Data from SC-XRD recorded at 100(2) K. [b] Average of three independent measurements and their standard deviations in brackets or after ± sign. [c] Calculated using BDE and ΔS° obtained from the van't Hoff plot at a temperature of 298.15 K. [d] Data from UV-Vis spectra measured in THF. [e] Calculated using the Eyring plot at a temperature of 298.15 K. [f] Values for each crystallographically independent molecule in the unit cell.

Conclusions

We reported direct observation of Co–Co bond homolysis using 2D EXSY NMR. The unambiguous observation of this process was supported by variable temperature NMR, EPR, and UV-Vis measurements and a series of control experiments, including unprecedented characterization of the dimeric and monomeric species by 2D DOSY NMR. 2D EXSY NMR characterization of Co–Co bond homolysis of $[Co(NHC)(CO)_3]_2$ complexes enabled us to study ligand steric and electronic effects that influence Co–Co bond strength. This study revealed that Co–Co bonds in $[Co(NHC)(CO)_3]_2$ complexes are weakened by steric bulk as well as electron donation. The observed electronic effect was explained based on the stabilization of the electron-deficient formal 17-electron species by an electron-donating ligand. We expect that the observed steric and electronic effects on Co–Co bond strength are applicable to designing other multimetallic complexes with various metal–metal bond strengths for applications including catalysis and materials chemistry.

Data availability

All experimental data associated with this work are available in the ESI.†

Author contributions

S. T. conceived the research program, synthesized, and characterized NHC ligands and complexes, discovered the 2D EXSY NMR observation, collected SC-XRD data, and conducted experiments to elucidate the thermodynamic and kinetic parameters. R. R. F analyzed the SC-XRD data and wrote the SC-XRD part of the ESI.† R. B. synthesized the precursors of NHC ligands. S. T. wrote the manuscript with revisions provided by the other authors.

Conflicts of interest

There are no conflicts to declare.

Acknowledgements

This research was supported by the Japan Society for the Promotion of Science (18K14230 and 22K05134, S. T.). This work was supported by Okinawa Institute of Science and Technology Graduate University instrumental analysis and engineering sections. S. T. thanks Dr Hajime Sato (Bruker Japan) for assistance with the 2D DOSY NMR measurement. R. R. F. performed crystal structure determination within the government statements for the Kazan Scientific Center of RAS.

Notes and references

1 *Encyclopedia of radicals in chemistry, biology, and materials*, ed. C. Chatgilialoglu and A. Studer, Wiley, Hoboken, 2014.
2 A. Studer and D. P. Curran, *Angew. Chem., Int. Ed.*, 2016, **55**, 58–102.
3 J. Stubbe and D. G. Nocera, *J. Am. Chem. Soc.*, 2021, **143**, 13463–13472.
4 K. J. Romero, M. S. Galliher, D. A. Pratt and C. R. J. Stephenson, *Chem. Soc. Rev.*, 2018, **47**, 7851–7866.
5 Y. Gao, D. Zhou, J. Lyu, S. A, Q. Xu, B. Newland, K. Matyjaszewski, H. Tai and W. Wang, *Nat. Rev. Chem.*, 2020, **4**, 194–212.
6 M. Abe, *Chem. Rev.*, 2013, **113**, 7011–7088.
7 D. Sakamaki, S. Ghosh and S. Seki, *Mater. Chem. Front.*, 2019, **3**, 2270–2282.
8 D. Griller and K. U. Ingold, *Acc. Chem. Res.*, 1976, **9**, 13–19.
9 C. D. Hoff, *Coord. Chem. Rev.*, 2000, **206–207**, 451–467.
10 R. G. Hicks, *Org. Biomole. Chem.*, 2007, **5**, 1321–1338.
11 J. Halpern and M. Pribanic, *Inorg. Chem.*, 1970, **9**, 2616–2618.
12 S. J. McLain, *J. Am. Chem. Soc.*, 1988, **110**, 643–644.
13 I. Kuksis and M. C. Baird, *Organometallics*, 1996, **15**, 4755–4762.
14 T. R. Dugan, E. Bill, K. C. MacLeod, G. J. Christian, R. E. Cowley, W. W. Brennessel, S. Ye, F. Neese and P. L. Holland, *J. Am. Chem. Soc.*, 2012, **134**, 20352–20364.
15 J. M. Wittman, R. Hayoun, W. Kaminsky, M. K. Coggins and J. M. Mayer, *J. Am. Chem. Soc.*, 2013, **135**, 12956–12959.
16 D. C. Lacy, G. M. Roberts and J. C. Peters, *J. Am. Chem. Soc.*, 2015, **137**, 4860–4864.
17 K. Uchida, Z. Mou, M. Kertesz and T. Kubo, *J. Am. Chem. Soc.*, 2016, **138**, 4665–4672.
18 B. Liu, T. Yoshida, X. Li, M. Stępień, H. Shinokubo and P. J. Chmielewski, *Angew. Chem., Int. Ed.*, 2016, **55**, 13142–13146.

19 T. Kobashi, D. Sakamaki and S. Seki, *Angew. Chem., Int. Ed.*, 2016, **55**, 8634–8638.
20 N. M. Bonanno, P. K. Poddutoori, K. Sato, K. Sugisaki, T. Takui, A. J. Lough and M. T. Lemaire, *Chem.– Eur. J.*, 2018, **24**, 14906–14910.
21 B. Adinarayana, D. Shimizu, K. Furukawa and A. Osuka, *Chem. Sci.*, 2019, **10**, 6007–6012.
22 B. Adinarayana, K. Kato, D. Shimizu, T. Tanaka, K. Furukawa and A. Osuka, *Angew. Chem., Int. Ed.*, 2020, **59**, 4320–4323.
23 W. C. Watkins, T. Jaeger, C. E. Kidd, S. Fortier, M. C. Baird, G. Kiss, G. C. Roper and C. D. Hoff, *J. Am. Chem. Soc.*, 1992, **114**, 907–914.
24 Y. Sunada, S. Ishida, F. Hirakawa, Y. Shiota, K. Yoshizawa, S. Kanegawa, O. Sato, H. Nagashima and T. Iwamoto, *Chem. Sci.*, 2016, **7**, 191–198.
25 E. L. Muetterties, B. A. Sosinsky and K. I. Zamaraev, *J. Am. Chem. Soc.*, 1975, **97**, 5299–5300.
26 W. P. Neumann, A. Penenory, U. Stewen and M. Lehnig, *J. Am. Chem. Soc.*, 1989, **111**, 5845–5851.
27 B. B. Wayland, A. E. Sherry, G. Poszmik and A. G. Bunn, *J. Am. Chem. Soc.*, 1992, **114**, 1673–1681.
28 V. Zaitsev, S. V. Rosokha, M. Head-Gordon and J. K. Kochi, *J. Org. Chem.*, 2006, **71**, 520–526.
29 J. P. Peterson, M. R. Geraskina, R. Zhang and A. H. Winter, *J. Org. Chem.*, 2017, **82**, 6497–6501.
30 B. B. Wayland, V. L. Coffin and M. D. Farnos, *Inorg. Chem.*, 1988, **27**, 2745–2747.
31 L. Y. Goh, S. K. Khoo and Y. Y. Lim, *J. Organomet. Chem.*, 1990, **399**, 115–123.
32 R. J. Klingler and J. W. Rathke, *J. Am. Chem. Soc.*, 1994, **116**, 4772–4785.
33 D. C. Woska, Y. Ni and B. B. Wayland, *Inorg. Chem.*, 1999, **38**, 4135–4138.
34 A. G. Bunn, Y. Ni, M. Wei and B. B. Wayland, *Inorg. Chem.*, 2000, **39**, 5576–5578.
35 E. F. van der Eide, T. Liu, D. M. Camaioni, E. D. Walter and R. M. Bullock, *Organometallics*, 2012, **31**, 1775–1789.
36 G. H. Imler, M. J. Zdilla and B. B. Wayland, *Inorg. Chem.*, 2013, **52**, 11509–11513.
37 G. Nocton, W. W. Lukens, C. H. Booth, S. S. Rozenel, S. A. Medling, L. Maron and R. A. Andersen, *J. Am. Chem. Soc.*, 2014, **136**, 8626–8641.
38 K. Lekin, S. M. Winter, L. E. Downie, X. Bao, J. S. Tse, S. Desgreniers, R. A. Secco, P. A. Dube and R. T. Oakley, *J. Am. Chem. Soc.*, 2010, **132**, 16212–16224.
39 K. Lekin, H. Phan, S. M. Winter, J. W. L. Wong, A. A. Leitch, D. Laniel, W. Yong, R. A. Secco, J. S. Tse, S. Desgreniers, P. A. Dube, M. Shatruk and R. T. Oakley, *J. Am. Chem. Soc.*, 2014, **136**, 8050–8062.
40 A. Dragulescu-Andrasi, A. S. Filatov, R. T. Oakley, X. Li, K. Lekin, A. Huq, C. Pak, S. M. Greer, J. McKay, M. Jo, J. Lengyel, I. Hung, E. Maradzike, A. E. DePrince, S. A. Stoian, S. Hill, Y.-Y. Hu and M. Shatruk, *J. Am. Chem. Soc.*, 2019, **141**, 17989–17994.
41 J. Zhang, D. C. Grills, K.-W. Huang, E. Fujita and R. M. Bullock, *J. Am. Chem. Soc.*, 2005, **127**, 15684–15685.
42 W. Li, X. Zhou, R. Lock, S. Patchkovskii, A. Stolow, C. Kapteyn Henry and M. Murnane Margaret, *Science*, 2008, **322**, 1207–1211.
43 H. J. Wörner, J. B. Bertrand, D. V. Kartashov, P. B. Corkum and D. M. Villeneuve, *Nature*, 2010, **466**, 604–607.
44 J. P. Lomont and C. B. Harris, *Inorg. Chim. Acta*, 2015, **424**, 38–50.
45 S. Yoshidomi, M. Mishima, S. Seyama, M. Abe, Y. Fujiwara and T.-a. Ishibashi, *Angew. Chem., Int. Ed.*, 2017, **56**, 2984–2988.
46 J. Jeener, B. H. Meier, P. Bachmann and R. R. Ernst, *J. Chem. Phys.*, 1979, **71**, 4546–4553.
47 C. L. Perrin and T. J. Dwyer, *Chem. Rev.*, 1990, **90**, 935–967.
48 K. Nikitin and R. O'Gara, *Chem.– Eur. J.*, 2019, **25**, 4551–4589.
49 P. Hamm, M. Lim and R. M. Hochstrasser, *J. Phys. Chem. B*, 1998, **102**, 6123–6138.
50 J. Zheng, K. Kwak and M. D. Fayer, *Acc. Chem. Res.*, 2007, **40**, 75–83.
51 J. P. Kraack, *Top. Curr. Chem.*, 2017, **375**, 86.
52 L. M. Kiefer and K. J. Kubarych, *Coord. Chem. Rev.*, 2018, **372**, 153–178.
53 C. R. Baiz, R. McCanne and K. J. Kubarych, *J. Am. Chem. Soc.*, 2009, **131**, 13590–13591.
54 R. Kania, A. I. Stewart, I. P. Clark, G. M. Greetham, A. W. Parker, M. Towrie and N. T. Hunt, *PCCP*, 2010, **12**, 1051–1063.
55 S. Rösel, C. Balestrieri and P. R. Schreiner, *Chem. Sci.*, 2017, **8**, 405–410.
56 S. Takebayashi and R. R. Fayzullin, *Organometallics*, 2021, **40**(4), 500–507.
57 M. Mayr, K. Wurst, K.-H. Ongania and M. R. Buchmeiser, *Chem.– Eur. J.*, 2004, **10**, 1256–1266.
58 M. Iglesias, D. J. Beetstra, A. Stasch, P. N. Horton, M. B. Hursthouse, S. J. Coles, K. J. Cavell, A. Dervisi and I. A. Fallis, *Organometallics*, 2007, **26**, 4800–4809.
59 J. J. Dunsford, K. J. Cavell and B. M. Kariuki, *Organometallics*, 2012, **31**, 4118–4121.
60 A. Gómez-Suárez, D. J. Nelson and S. P. Nolan, *Chem. Commun.*, 2017, **53**, 2650–2660.
61 A. Kumar, D. Yuan and H. V. Huynh, *Inorg. Chem.*, 2019, **58**, 7545–7553.
62 P. N. Bungu and S. Otto, *Dalton Trans.*, 2011, **40**, 9238–9249.
63 J. Du, W. Chen, Q. Chen, X. Leng, Y.-S. Meng, S. Gao and L. Deng, *Organometallics*, 2020, **39**, 729–739.
64 H. B. Abrahamson, C. C. Frazier, D. S. Ginley, H. B. Gray, J. Lilienthal, D. R. Tyler and M. S. Wrighton, *Inorg. Chem.*, 1977, **16**, 1554–1556.
65 M. P. Crockett, H. Zhang, C. M. Thomas and J. A. Byers, *Chem. Commun.*, 2019, **55**, 14426–14429.
66 R. Dorta, E. D. Stevens, C. D. Hoff and S. P. Nolan, *J. Am. Chem. Soc.*, 2003, **125**, 10490–10491.
67 S. Goebel, C. L. Haynes, F. A. Khan and P. B. Armentrout, *J. Am. Chem. Soc.*, 1995, **117**, 6994–7002.
68 G. G. Christoph and Y. B. Koh, *J. Am. Chem. Soc.*, 1979, **101**, 1422–1434.
69 I. G. Powers and C. Uyeda, *ACS Catal.*, 2017, **7**, 936–958.
70 J. Campos, *Nat. Rev. Chem.*, 2020, **4**, 696–702.

71 J. F. Berry and C. C. Lu, *Inorg. Chem.*, 2017, **56**, 7577–7581.
72 R. J. Hoobler, M. A. Hutton, M. M. Dillard, M. P. Castellani, A. L. Rheingold, A. L. Rieger, P. H. Rieger, T. C. Richards and W. E. Geiger, *Organometallics*, 1993, **12**, 116–123.
73 G. W. Margulieux, N. Weidemann, D. C. Lacy, C. E. Moore, A. L. Rheingold and J. S. Figueroa, *J. Am. Chem. Soc.*, 2010, **132**, 5033–5035.
74 D. W. Agnew, C. E. Moore, A. L. Rheingold and J. S. Figueroa, *Angew. Chem., Int. Ed.*, 2015, **54**, 12673–12677.
75 R. H. Duncan Lyngdoh, H. F. Schaefer and R. B. King, *Chem. Rev.*, 2018, **118**, 11626–11706.
76 L. D. Brown, K. N. Raymond and S. Z. Goldberg, *J. Am. Chem. Soc.*, 1972, **94**, 7664–7674.
77 F. T. T. Ng, G. L. Rempel, C. Mancuso and J. Halpern, *Organometallics*, 1990, **9**, 2762–2772.
78 H. Clavier and S. P. Nolan, *Chem. Commun.*, 2010, **46**, 841–861.
79 D. J. Nelson and S. P. Nolan, *Chem. Soc. Rev.*, 2013, **42**, 6723–6753.
80 H. V. Huynh, *Chem. Rev.*, 2018, **118**, 9457–9492.
81 R. J. Klingler, M. J. Chen, J. W. Rathke and K. W. Kramarz, *Organometallics*, 2007, **26**, 352–357.
82 F. A. L. Anet, I. Yavari, I. J. Ferguson, A. R. Katritzky, M. Moreno-Mañas and M. J. T. Robinson, *J. Chem. Soc., Chem. Commun.*, 1976, 399–400, DOI: **10.1039/C39760000399**.